Report

Cell Reports

The C-Domain of the NAC Transcription Factor ANAC019 Is Necessary for pH-Tuned DNA Binding through a Histidine Switch in the N-Domain

Graphical Abstract

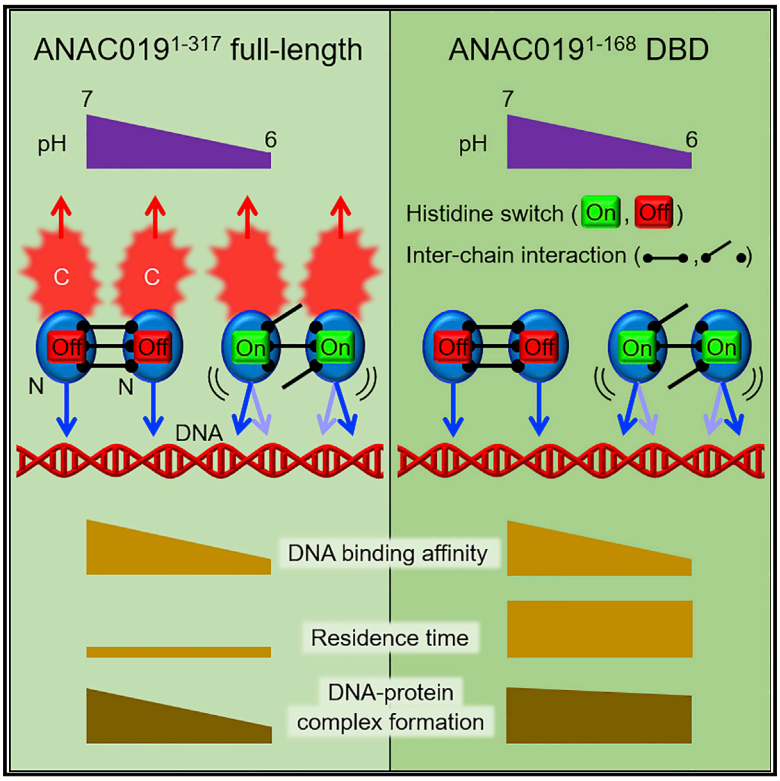

Authors

Mooseok Kang, Sangyeol Kim, Hyo Jung Kim, ..., Weontae Lee, Hong Gil Nam, Iksoo Chang

Correspondence

wlee@spin.yonsei.ac.kr (W.L.), nam@dgist.ac.kr (H.G.N.), iksoochang@dgist.ac.kr (I.C.)

In Brief

Kang et al. find a histidine switch in the DNA-binding N-domain of the transcription factor ANAC019 that regulates both pH-dependent homodimerization and DNA binding. They propose that long-range electrostatic interactions between DNA and the negatively charged C-terminal turns on the pH dependency of the DNA-binding affinity of the N-terminal DNA-binding domain.

Highlights

- The transcription factor ANAC019 has a histidine switch in its DNA-binding N-domain
- The histidine switch influences homodimerization and DNA binding
- The C-domain is required for the pH-dependent formation of a DNA-protein complex
- The C-domain determines the residence time near DNA via electrical interactions

Kang et al., 2018, Cell Reports 22, 1141–1150
January 30, 2018
https://doi.org/10.1016/j.celrep.2018.01.002

CellPress

Cell Reports
Report

The C-Domain of the NAC Transcription Factor ANAC019 Is Necessary for pH-Tuned DNA Binding through a Histidine Switch in the N-Domain

Mooseok Kang,[1,2,8] Sangyeol Kim,[1,2,8] Hyo Jung Kim,[3,8] Pravesh Shrestha,[4,8] Ji-hye Yun,[4] Bong-Kwan Phee,[3] Weontae Lee,[4,*] Hong Gil Nam,[3,5,*] and Iksoo Chang[1,6,7,9,*]
[1]Center for Proteome Biophysics, DGIST, Daegu 42988, Korea
[2]Department of Physics, Pusan National University, Busan 46241, Korea
[3]Center for Plant Aging Research, Institute for Basic Science, Daegu 42988, Korea
[4]Department of Biochemistry, Yonsei University, Seoul 03722, Korea
[5]Department of New Biology, DGIST, Daegu 42988, Korea
[6]Department of Brain and Cognitive Sciences, DGIST, Daegu 42988, Korea
[7]Core Protein Resources Center, DGIST, Daegu 42988, Korea
[8]These authors contributed equally
[9]Lead Contact
*Correspondence: wlee@spin.yonsei.ac.kr (W.L.), nam@dgist.ac.kr (H.G.N.), iksoochang@dgist.ac.kr (I.C.)
https://doi.org/10.1016/j.celrep.2018.01.002

SUMMARY

The affinity of transcription factors (TFs) for their target DNA is a critical determinant of gene expression. Whether the DNA-binding domain (DBD) of TFs alone can regulate binding affinity to DNA is an important question for identifying the design principle of TFs. We studied ANAC019, a member of the NAC TF family of proteins in *Arabidopsis*, and found a well-conserved histidine switch located in its DBD, which regulates both homodimerization and transcriptional control of the TF through H135 protonation. We found that the removal of a C-terminal intrinsically disordered region (IDR) in the TF abolished the pH-dependent binding of the N-terminal DBD to DNA. We propose a mechanism in which long-range electrostatic interactions between DNA and the negatively charged C-terminal IDR turns on the pH dependency of the DNA-binding affinity of the N-terminal DBD.

INTRODUCTION

Transcriptional control by transcription factors (TFs) is a fundamental cellular regulatory mechanism (Spitz and Furlong, 2012). One of the key molecular mechanisms of transcriptional control is the regulation of the binding affinity of TFs to their target DNA, which responds to intra- and extracellular conditions. Indeed, the binding affinity is often controlled by protein modifications, such as phosphorylation (Filtz et al., 2014), oxidation, glycosylation, and protonation (Mikles et al., 2013). The conformational changes that typically occur in the conserved DNA-binding domain (DBD) of a TF can influence the dimerization of TFs and DNA binding (Müller, 2001). The other TF domains, which are frequently intrinsically disordered, are responsible for transcriptional activation, repression, and binding to multiple proteins (Bista et al., 2012). The functional modularity of each domain of a TF seems to act independently in many TFs (Kragelund et al., 2012). However, whether the functional modularity of the DBD alone (i.e., without the disordered domains) is sufficient to regulate its binding affinity to DNA following changes in cellular conditions has been unclear. Although the disordered domain has its own function, an important question remains: Is the disordered domain itself necessary to turn on the functional modularity of the DBD? Indeed, whether the disordered domains regulate the functional modularity of the DBD in response to changes in cellular conditions and the possible mechanism of this regulation have not been well studied. Therefore, it is critical to investigate the design principle behind the functional modularity of two-domain TFs as it relates to transcriptional control following changes in cellular conditions.

For our studies, we chose NAC (no apical meristem [NAM], Arabidopsis transcription activation factor [ATAF], and cup-shaped cotyledon [CUC]), a key plant TF family. In *Arabidopsis*, 108 NAC TF proteins control the many essential aspects of plant development and environmental responses (Ooka et al., 2003). They are composed of a highly conserved N-terminal DBD and divergent C-terminal intrinsically disordered region (IDR) (Figure S1) (Ernst et al., 2004). Similar to many other TFs, NAC TFs can form homo- and heterodimers with the N-terminal DBDs and bind to DNA in a dimeric form (Welner et al., 2012). While studying the function of NAC TFs in plant development and environmental stresses (Jensen et al., 2010; Kim et al., 2009), we observed a conserved histidine residue in the N-terminal DBD among 80% of the 108 NAC TF proteins (Figure S2A). Although there are established functional modularity for the C-terminal IDR of NAC TFs (Kragelund et al., 2012), the ability of the C-terminal IDR to influence the DNA-binding affinity of the N-terminal DBD of NAC TFs in response to changes in cellular conditions is not known.

In this study, we selected ANAC019 TF as our test TF, because its dimeric three-dimensional structure of the N-terminal DBD

region ANAC019$^{1–168}$ (ANAC019$^{1–168}$ DBD) was known (Ernst et al., 2004). We investigated the role of its conserved histidine in the dimerization of ANAC019 monomers and the role of the C-terminal IDR, ANAC019$^{169–317}$, in the regulation of the DNA-binding affinity of the ANAC019$^{1–168}$ DBD to its target DNA in response to changes in cellular pH. Our study included both *in vitro* and *in vivo* experiments and *in silico* simulations. We demonstrated that a single histidine residue, H135, which is located in the ANAC019$^{1–168}$ DBD, acts as a histidine switch and regulates both the pH-dependent dimerization of ANAC019$^{1–168}$ DBD monomers and the pH-dependent transcriptional control of the binding of the ANAC019 TF dimer to its target DNA. In contrast, removal of the C-terminal IDR from the ANAC019 TF abolished the pH dependency of the DNA-binding affinity of the ANAC019$^{1–168}$ DBD. We propose that a long-range electrostatic interaction between DNA and the negatively charged C-terminal IDRs of the ANAC019 TF dimer promotes the pH dependency of the DNA-binding affinity of the positively charged N-terminal DBD. We suggest that the functional modularity of the N-terminal DBD of the TF itself may not always be sufficient for its transcriptional control following cellular pH changes. Thus, the negatively charged C-terminal IDR is necessary for turning on the pH dependency of the DNA-binding affinity of the N-terminal DBD.

RESULTS

ANAC019$^{1–168}$ DBD Structure Depends on H135 Protonation Status

The three-dimensional structure of a monomer of the ANAC019$^{1-168}$ DBD, determined previously by X-ray crystallography (PDB: 1UT4 and PDB: 1UT7) (Ernst et al., 2004) with missing structures for flexible loops, was reconstructed by MODELER and used for all-atom molecular dynamics (MD) simulations of an ANAC019$^{1–168}$ DBD homodimer (Supplemental Experimental Procedures). The backbone structures of 50 reconstructed monomers were superimposed (Figure 1A, left) and showed that a twisted antiparallel beta-sheet was packed against an N-terminal alpha helix ($\alpha 1$) from D24 to A36 and a short alpha helix ($\alpha 2$) from P56 to K62. Flexible loops connected these secondary structures. The side chain of an unprotonated H135 was mostly exposed to the solvent, and H135 does not form an intra-chain salt bridge with D24 (the HD-off state) (Figure 1A, left). We performed the additional MD simulations and the numerical calculation for estimating pKa value of H135, which is ~6.7 (Figures S2B and S2C). MD simulations generated 50 structural ensembles for a monomer of ANAC019$^{1–168}$ DBD with a protonated H135, resulting in the emergence of an intra-chain salt bridge between the protonated H135 and D24 (the HD-on state) (Figure 1A, right). The atomic arrangements for the HD-off and HD-on states are presented in Figure 1B, left and right, respectively. The protonation of H135 promoted more occupancy of the hydrogen bonds for not only D24-H135 but also D24-R158 and E25-K114, causing a shift of the axis of the $\alpha 1$-helix toward the twisted antiparallel beta sheet (Figure 1B). The change in the chemical shift of D24 obtained by two-dimensional $^{1}H/^{15}N$ heteronuclear single quantum coherence (HSQC) nuclear magnetic resonance (NMR) for ^{15}N labeled ANAC019$^{1-168}$ DBD was appreciable when the pH decreased from 7.5 to 6.0, reflecting a change in the structural environment of D24, whereas that of H135 was relatively negligible (Figure 1C).

The biological significance of the structural shift in ANAC019 was tested by comparing the transactivation assay of ANAC019 with its mutant, ANAC019^{H135K}, using *Arabidopsis* mesophyll protoplast cells (Figure 1D). Plant protoplasts without cell walls offer a versatile cell-based experimental system, but they are very fragile. Protoplasts still function as intact cells. The intracellular pH of typical plant cells is kept mostly homeostatic, and there is no report on a facile way of arbitrarily changing intracellular pH of plant cells. We thus examined the effect ANAC019^{H135K} on the activation of a target gene, where lysine mimics a protonated form of the imidazole side-chain histidine (Welner et al., 2012). The comparison was made toward a reporter construct containing the firefly luciferase (LUC) reporter gene under the control of the ANAC083 promoter (pANAC083-LUC), a target of ANAC019 previously found in our lab (Figure 1E). The luciferase activity was significantly increased when pANAC083-LUC was co-transfected with 35Sp:ANAC019 hemagglutinin (HA), whereas ANAC019^{H135K}-HA showed little increased transactivation capacity over the control. This indicates that the protonation status of H135 critically affects the activation of downstream target gene.

Effect of H135 Protonation on the Dimerization of ANAC019 Monomers

NAC TFs become active following dimerization. The ANAC019 homodimer is formed by the N-terminal DBDs. Based on 50 structures of the HD-off monomer state (Figure 1A, left), the protein-protein docking test for 1,275 pairs of two ANAC019$^{1–168}$ DBDs showed that ~81% of the dimer candidates maintained the interchain hydrogen bond interactions across the dimeric interface (Experimental Procedures). In contrast, only 2% of the dimer candidates maintained the interchain hydrogen bond interactions across the dimeric interface in the HD-on monomer state. These data suggest that the HD-off state of an ANAC019$^{1–168}$ DBD monomer is more likely to form a functional dimer, and therefore the protonation status of H135 could play a pivotal role in the regulation of the dimerization of ANAC019$^{1–168}$ DBDs.

We performed co-immunoprecipitation assays using wild-type ANAC019 and mutant ANAC019^{H135K} in plant cells. As presented in Figure 2A, wild-type pairs (ANAC019-HA and ANAC019-GFP) showed more binding than the mutant pairs (ANAC019^{H135K}-HA and ANAC019^{H135K}-GFP). The same trend persisted for the dimeric interaction between ANAC019$^{1–168}$ DBDs (Figure 2B). These results were consistent with those obtained using the yeast two-hybrid assay (Figure 2C) and indirectly supported the hypothesis that the protonation of H135 reduces the degree of dimerization.

Size exclusion chromatography of the ANAC019$^{1–168}$ DBD in a solution environment demonstrated that ANAC019$^{1–168}$ DBD was mostly present as a dimer or monomer in a buffer of 140 or 57 mM NaCl, respectively, at both pH 7.5 and 6.0 (Figures 2D and 2F, respectively). In 70 mM NaCl, we observed that the composition of dimer is higher at pH 7.5 than at pH 6.0, and

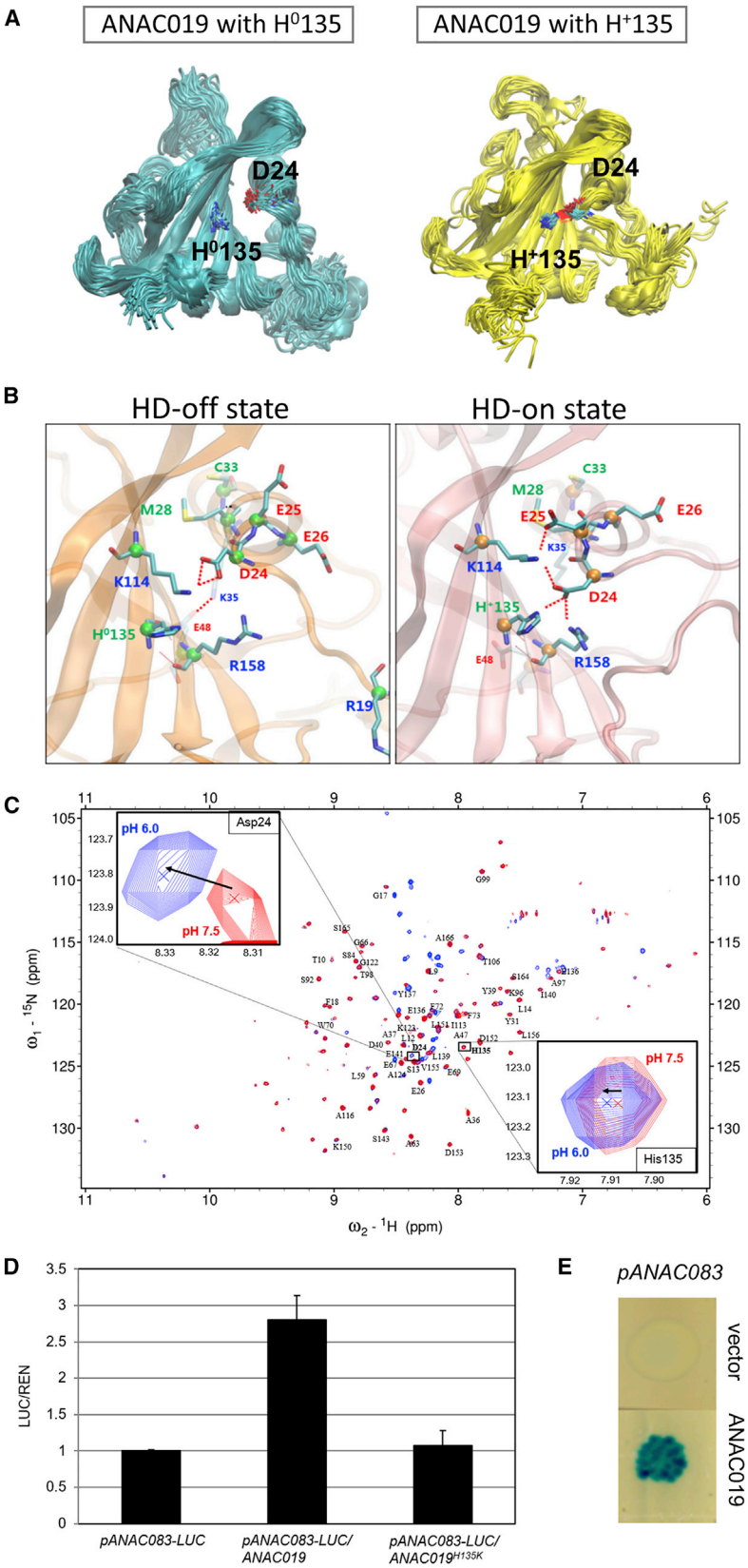

Figure 1. H135 in a Monomer of ANAC019$^{1–168}$ DBD Mediates Protonation-Dependent Conformational Change from the HD-Off to HD-On State

(A) Fifty superimposed backbone structures of the ANAC019$^{1–168}$ DBD from MD simulations when H135 was unprotonated (left) and protonated (right) in the absence (HD-off state) and presence (HD-on state) of an intrachain salt bridge between D24 and H135.

(B) Atom-level structural arrangement when H135 was unprotonated so that an intrachain salt bridge between H135 and D24 is absent (i.e., HD-off state) (left) and when H135 was protonated so that an intrachain salt bridge between H135 and D24 is present (i.e., HD-on state) (right).

(C) Superposition of two-dimensional $^{1}H/^{15}N$ HSQC spectra of ^{15}N-labeled ANAC019$^{1–168}$ DBD at pH 7.5 (red) and pH 6.0 (blue) with the 20 mM NaPi, 140 mM NaCl and 0.5 mM DTT, and 0.01% NaN3 conditions.

(D) Luciferase activity of the *ANAC083* promoter by ANAC019 and a mutant ANAC019^{H135K}.

(E) Yeast one-hybrid assay between ANAC019 and the ANAC083 promoter. ANAC019 prey vector or empty vector (negative control) was introduced into yeast cells along with the ANAC083 promoter. The growth of a blue yeast colony on selective medium containing X-gal indicates a positive interaction.

See also Figures S2 and S3 and Table S1.

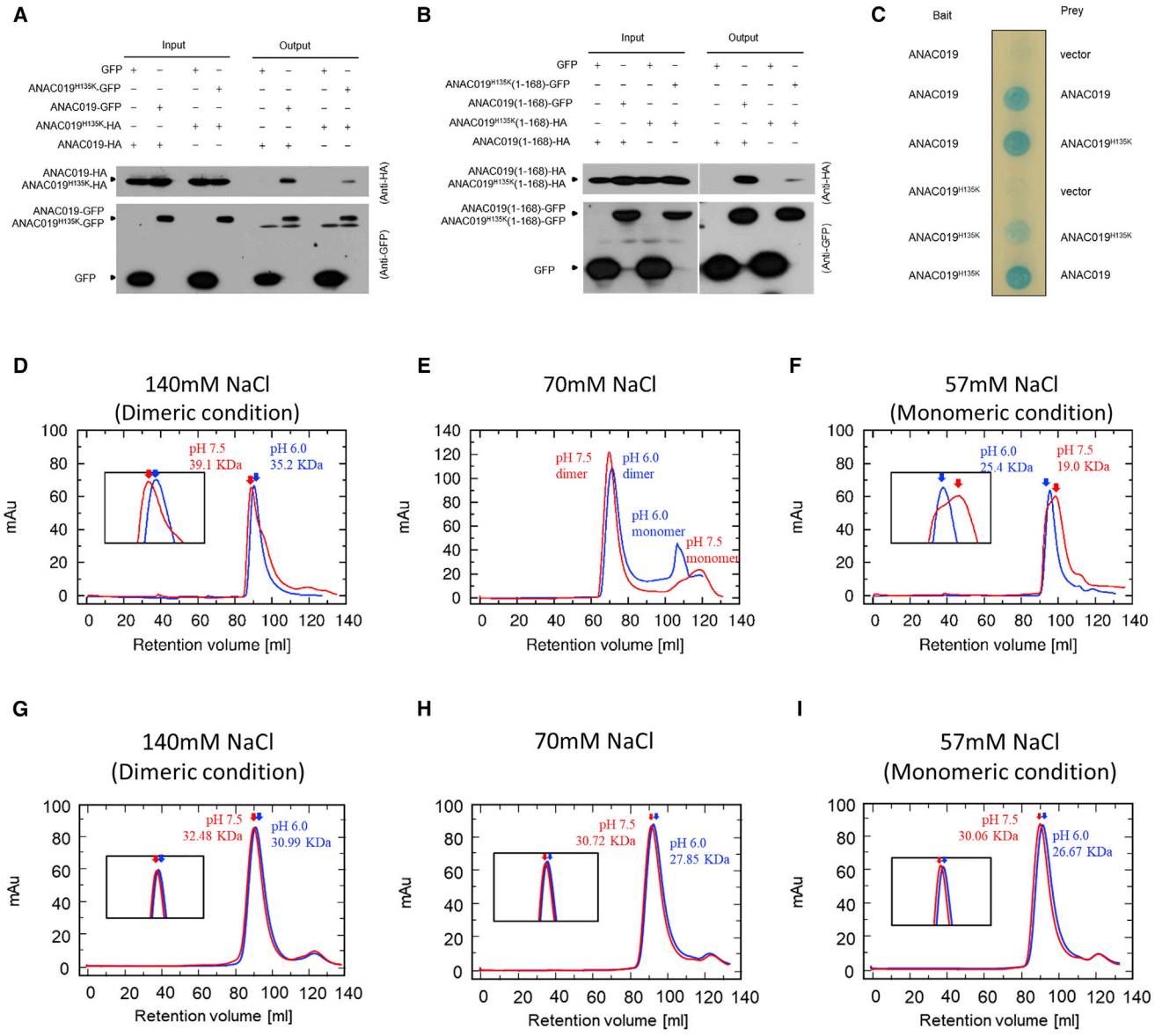

Figure 2. Effect of H135 Protonation on Dimerization of ANAC019$^{1–168}$ DBD and ANAC019$^{1–317}$ Full Length

(A and B) Co-immunoprecipitation assay using wild-type and mutant ANAC019^{H135K} in the dimerization of full-length ANAC019$^{1–317}$ (A) or ANAC019$^{1–168}$ DBD (B). Protoplast cells were cotransfected with ANAC019$^{1–317}$-HA, ANAC019^{H135K}-HA, ANAC019$^{1–168}$ DBD-HA, or ANAC019^{H135K} DBD-HA along with either its GFP-tagged one or a GFP control. The GFP-tagged or GFP proteins were immunoprecipitated with an anti-GFP antibody, and an immunoblot was probed with anti-HA and anti-GFP antibodies.

(C) Mutation of histidine to lysine affects dimerization of ANAC019 in yeast. Pairs of indicated bait and prey vectors were transformed into yeast cells. The growth of a blue yeast colony on selective medium containing X-gal indicates a positive interaction.

(D–F) Size exclusion chromatography of ANAC019$^{1–168}$ DBD using Superdex 200 (D and F) and Superdex 75 (E). The elution profiles for pH 7.5 (red line) and 6.0 (blue line) at 140 mM (D), 70 mM (E), or 57 mM NaCl (F). Effect of H135K mutation on dimerization of the N-terminal DBD of ANAC019.

(G–I) Size exclusion chromatography of ANAC019^{H135K} DBD using Superdex 200. The elution profiles for pH 7.5 (red line) and 6.0 (blue line) at 140 mM (G), 70 mM (H), and 57 mM (I) NaCl are shown.

the monomer composition was lower at pH 7.5 than at pH 6.0 (Figure 2E). However, the migration profile for pH 7.5 is slightly different from that for pH 6.0 due to relative population of protonation state of H135 (Figures 2D and 2E). The elution profiles of monomer for pH 7.5 and pH 6.0 are also affected by the protonation state of H135. We think the migration profile of the gel-filtration chromatography for different pH environments is mostly modulated by either local or global structural changes in ANAC019$^{1–168}$ DBD due to charge distribution and/or the hydrogen bonding network. Our hypothesis was confirmed by elution profiles from the additional experiments for the H135K mutant, which does not influence elution profile much

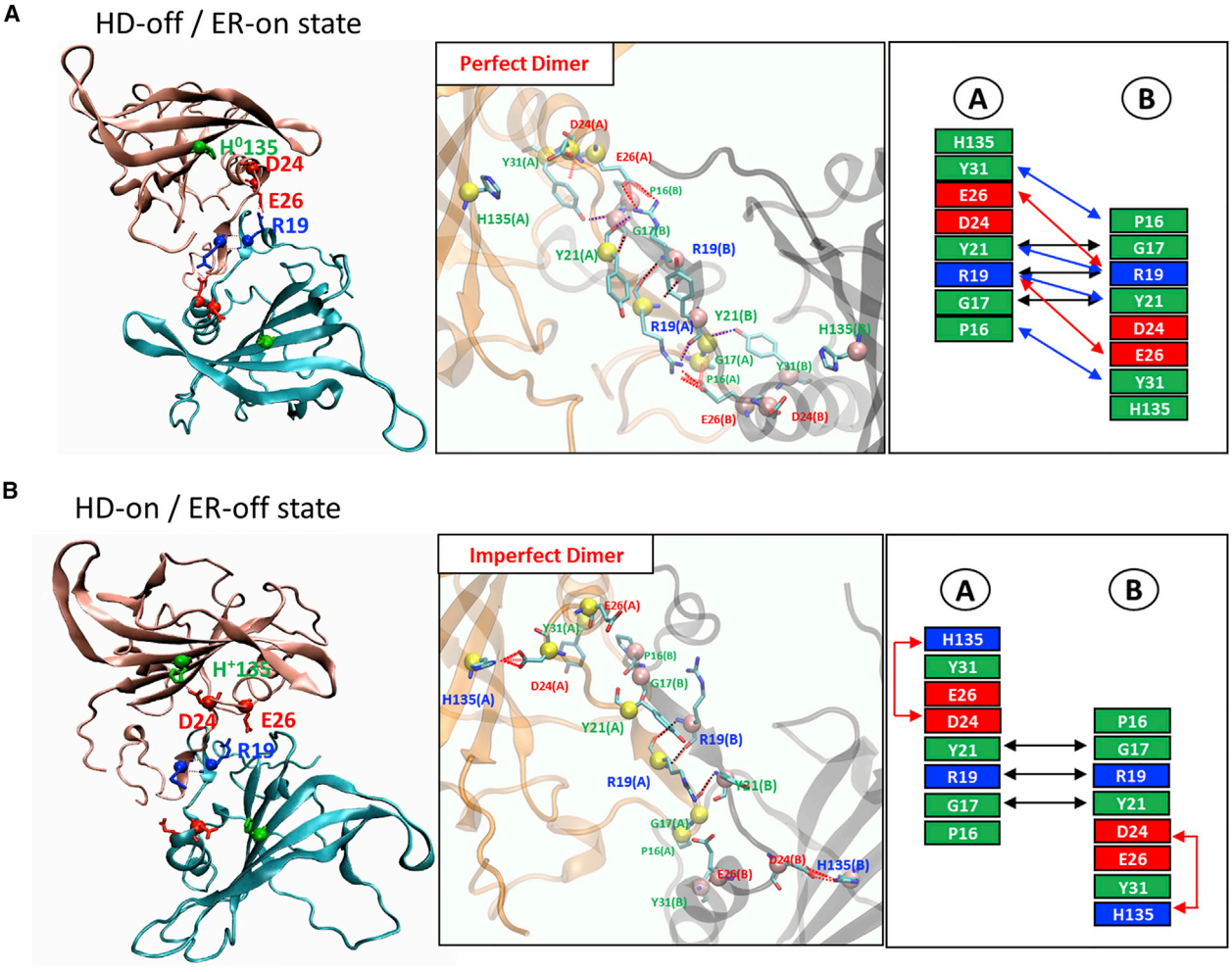

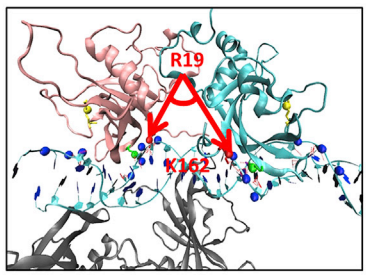

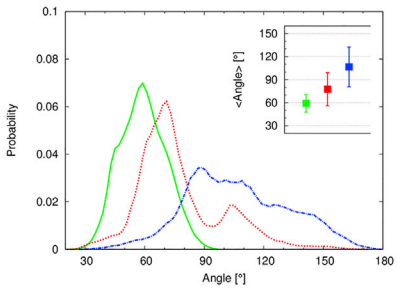

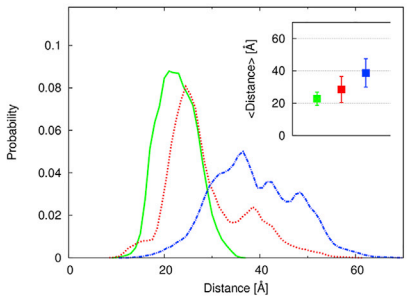

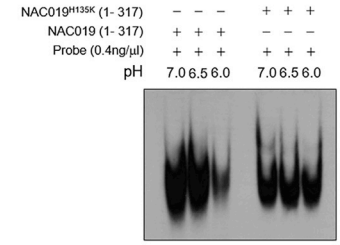

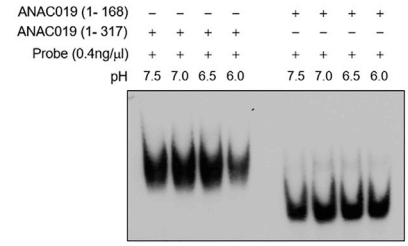

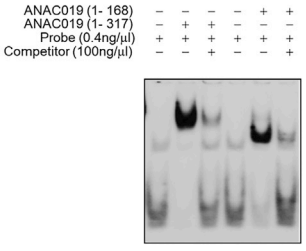

(legend on next page)

(Figures 2G–2I). It is, therefore, possible that H135 protonation is reflected by the relative differences in these elution profiles. Since the ANAC019 TF binds to DNA as a dimer, the very nature of the structural versatility in a dimer of the ANAC019$^{1–168}$ DBD that is dependent on the intracellular pH is of high significance for this gene regulatory system (Olsen et al., 2004; Welner et al., 2012).

ANAC019$^{1–168}$ DBD Dimer Structure Depends on the H135 Protonation State

We performed extensive MD simulations to generate structural ensembles for a dimer of the ANAC019$^{1–168}$ DBD or the ANAC019$^{1–317}$ full-length (Figure S3; Table S1). This analysis revealed that the presence of a perfect or imperfect dimer state depends on the H135 protonation state. The perfect dimer state (Figure 3A) is characterized by the forearm shake configuration, where its binding interface is characterized by both an interchain antiparallel beta sheet formed by backbone hydrogen bond interactions between the F^{18}R^{19}F^{20} (A chain) and F^{20}R^{19}F^{18} (B chain) residues and two interchain salt bridges formed by a side-chain hydrogen bond interactions between R^{19} (A chain) and E^{26} (B chain) (the ER-on state) and vice versa the HD-off/ER-on state). The protonation of H135 not only induced an intrachain salt bridge between H135 and D24 but also shifted the $\alpha 1$-helix containing the D24, E25, and E26 residues toward an intrachain antiparallel beta sheet, which then breaks down all or any one of two interchain salt bridges between E26 and R19 (the ER-off state). The imperfect ANAC019$^{1–168}$ DBD dimer state is characterized by the HD-on/ER-off state, while it still maintains backbone hydrogen bond interactions across the inter-chain antiparallel beta-sheet (Figure 3B). Along the trajectories of our MD simulations without H135 protonation, 95% of the structural snapshots maintained the HD-off/ER-on dimer state. In contrast, 87% of the structural snapshots preserved the HD-on/ER-off in MD simulations with H135 protonation. Therefore, it implicates that H135 plays the role of a histidine switch by forming a salt-bridge with D24 depending on its protonation status.

The qualitative propensity for an ANAC019 dimer to bind to DNA was evaluated using the fluctuation of both an opening angle formed by the K^{162}R^{19}K^{162} residues and an opening distance between the two K^{162}s of both chains in the DNA binding region (Figure 3C) (Welner et al., 2012). In the course of our MD simulations, we kept track the conformational fluctuations of ANAC019 dimer configurations along MD trajectories and calculated both an opening angle and an opening distance. The average of the dimer's opening angle for a complex of DNA-bound ANAC019$^{1–168}$ DBD dimer was ~60°, and the distance was 20 Å. However, this angle was 85° for a DNA-free perfect dimer of ANAC019$^{1–317}$ full-length with a distance of 25 Å and 105° for a DNA-free imperfect dimer of ANAC019$^{1–317}$ full-length with a broader distribution and a distance of 35 Å (Figures 3D and 3E). The shift between the perfect and the imperfect dimer distribution curves indicated that the degree of structural fluctuation across the dimer's interface in the HD-on/ER-off state was larger than that of the HD-off/ER-on state.

Effect of pH on DNA-Protein Complex Formation with Full-Length ANAC019 or ANAC019$^{1–168}$ DBD Dimers

Whether the complex formation between ANAC019 and its target DNA sequence is altered by H135 protonation was tested using the electrophoretic mobility shift assay (EMSA) at different pH levels. ANAC019 recombinant proteins were purified as dimers. We first checked the amount of full-length ANAC019 at different pH levels and found the amount of ANAC019 protein is little affected in different pH levels. As shown in Figure 3F, the complex formation between full-length ANAC019$^{1–317}$ and the target sequence was sensitive to pH. The amount of the DNA-ANAC019 complex was decreased as pH was lowered from pH 7.0 to 6.0, which indicates that the change in DNA-ANAC019 complex formation is pH dependent. In contrast, the complex formation between the ANAC019^{H135K} full-length mutant protein and the target sequence was minimally influenced by pH. However, DNA-protein complex formation with the mutant protein was reduced compared to that with the wild-type at pH 7.0 to 6.5 but higher at pH 6.0. These results indicate that the H135 located in the N-terminal DBD of full-length ANAC019$^{1–317}$ is a residue that determines the sensitivity to pH in DNA-protein complex formation. As shown in Figures 3D and 3E, as the area under a green distribution curve of an opening angle or distance, respectively, overlaps more with that of a red curve than a blue curve, the probability for an imperfect dimer of full-length ANAC019$^{1–317}$ to form a complex with a target DNA sequence is lower than that of a perfect ANAC019$^{1–317}$ full-length dimer. We also tested pH-sensitive DNA-protein complex formation with the N-terminal DBD of ANAC019. Surprisingly, DNA-protein complex formation

Figure 3. Effect of H135 Protonation on the Dimer State and Structural Fluctuation across the Dimeric Interface

(A and B) The structural arrangement across the binding interface of (A) a perfect dimer (HD-off/ER-on state) and (B) an imperfect dimer (HD-on/ER-off state). Colors of the arrows in the bottom panel represent the kinds of interactions: salt bridge (red), backbone-side chain (blue), and backbone-backbone (black) hydrogen bond interactions.

(C) An opening angle formed by the K^{162}R^{19}K^{162} residues and an opening distance between two K^{162}s in both chains of a dimeric ANAC019.

(D and E) The distributions of opening angle (D) and distance(E) for a complex of DNA-bound ANAC019$^{1–168}$ DBD dimer (green, averaged over 300,000 snapshots), a DNA-free perfect dimer of full-length ANAC019$^{1–317}$ (red, 222,087 snapshots), and a DNA-free imperfect dimer of full-length ANAC019$^{1–317}$ (blue, 336,228 snapshots). These were calculated by keeping track of the conformational fluctuations of ANAC019 dimer configurations in MD simulations. The inset shows the average opening angle and distance.

(F and G) Binding of full-length ANAC019$^{1–317}$ and full-length ANAC019^{H135K} (F) and ANAC019$^{1–168}$ DBD (G) to a synthetic oligonucleotide at different pH levels by EMSA.

(H) Analysis of the DNA-binding specificity of ANA019. The unlabeled competitor DNA fragment with the same wild-type sequence effectively diminished the binding of full-length ANAC019$^{1–317}$ or ANAC019$^{1–168}$ DBD to the labeled fragment.

See also Figure S3 and Table S1.

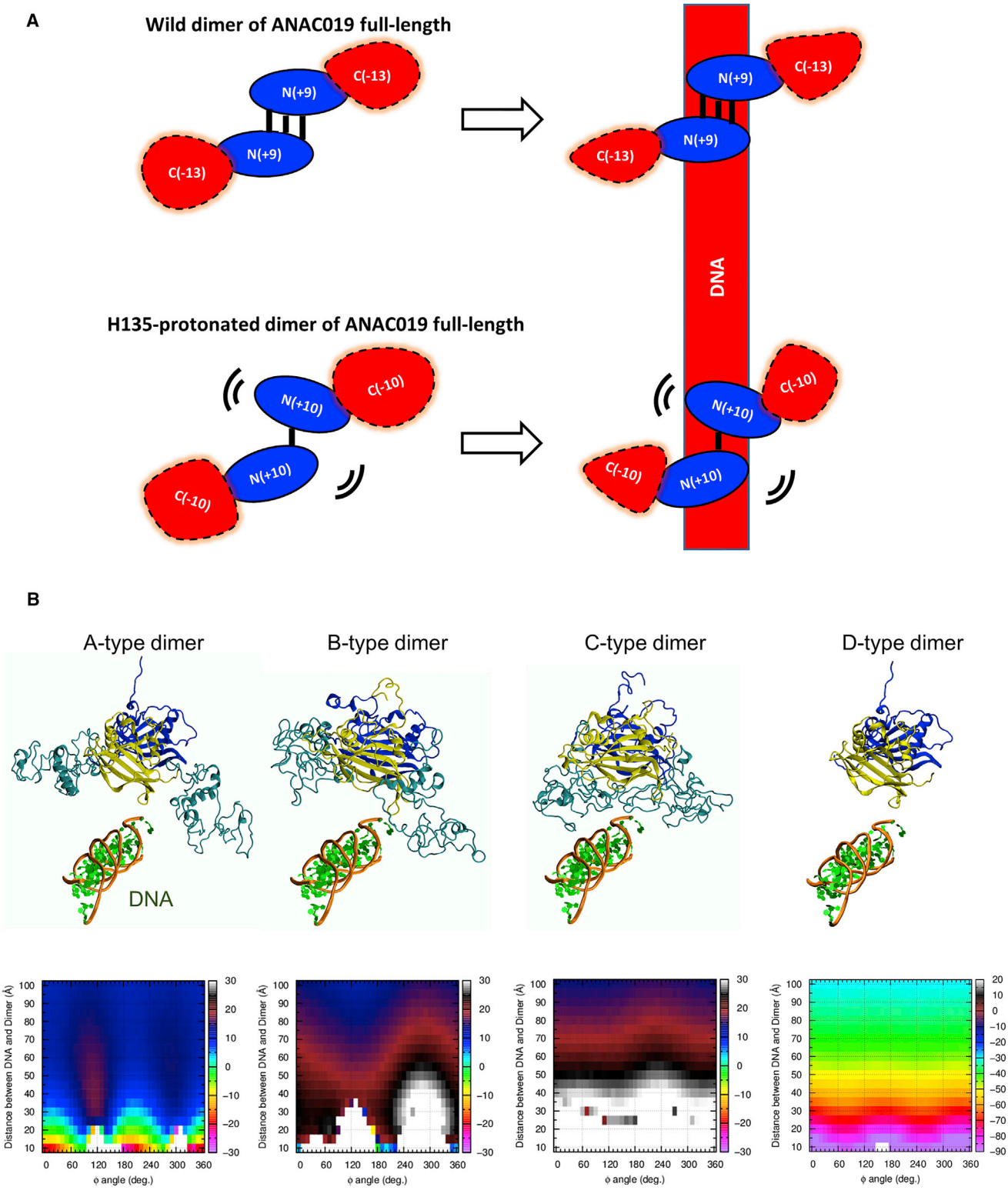

Figure 4. Schematics for the Interactions between ANAC019$^{1-317}$ Full-Length and DNA

(A) Full-length ANAC019$^{1-317}$ was electrostatically modeled as an electric dipole which points from the C-domain with a net charge of −13*e* to the N-terminal DBD with a net charge of +9*e*. DNA is considered to be a negatively charged rod. The structural ensembles of intrinsically disordered C terminus are denoted by the dotted line around its circumference.

(legend continued on next page)

between the ANAC019$^{1–168}$ DBD and a target sequence became insensitive to pH (Figure 3G), even though it still contained H135 and its binding was specific (Figure 3H).

Physical Role of Negatively Charged C-Terminal IDR of ANAC019

Our data raised the question of why the C-terminal domain (C-domain) of full-length ANAC019$^{1–317}$ was indispensable for the pH sensitivity of the binding of the ANAC019 N-terminal DBD to a target DNA sequence. The net charge of the wild-type ANAC019$^{1–168}$ DBD is +9*e*, whereas that of an H135-protonated ANAC019$^{1–168}$ DBD is +10*e*. In contrast, the net charge of full-length wild-type ANAC019$^{1–317}$ is −4*e*, whereas that of an H135-protonated full-length ANAC019$^{1–317}$ is 0*e*. An ANAC019$^{1–168}$ DBD dimer has a longer residency time near DNA than the full-length dimer, since it is strongly attracted to negatively charged DNA. In contrast, the ANAC019$^{1–317}$ full-length dimer is weakly repelled. Therefore, the degree of complex formation by an ANAC019$^{1–168}$ DBD dimer and DNA is insensitive to the protonation status of H135 within the time window of the experiment, which suggests that it is insensitive to pH (Figure 3G). In Figure 4A, we modeled ANAC019$^{1–317}$ full-length dimer binding in the distal situation as the attraction of two electric dipoles, while connected under the forearm shake configuration (Figure 3A), to a negatively charged DNA rod. The distance and relative orientation of a dimer of full-length ANAC019$^{1–317}$ to DNA are characterized by (d, θ, φ), where (θ, φ) = (0°, 0°) refers to the orientation in PDB: 3SWP (Figure S4). Since the C-domain takes various disordered configurations, three representative configurations were considered in our calculation depending on both the magnitude of the electric dipole moment and the extent of the exposure of the DBD in full-length ANAC019$^{1–317}$ to DNA (Figure 4B). The A-type dimer of full-length ANAC019$^{1–317}$, which had a large electric dipole moment and whose DBDs were fully exposed to DNA, experienced a strong d- and φ-dependent orientational selectivity in its binding to DNA (Figure 4B, bottom). The B- and C-type dimers had medium and small electric dipole moments, respectively, with only partial or minimal exposure to DNA. These conditions resulted in weak or minimal d- and φ-dependent orientational selectivity in their binding to DNA, respectively. Thus, the orientational selectivity was maximized when an A-type dimer bound to DNA by minimizing the electrostatic dipole potential energy in the electric field generated by the negatively charged DNA. In contrast, the D-type ANAC019$^{1–168}$ DBD dimer without the negatively charged C-terminal IDR showed little orientational sensitivity (Figure 4B, bottom right).

DISCUSSION

We found a histidine-switch H135-D24 located in the ANAC019$^{1–168}$ DBD, which is conserved among 80% of the 108 NAC TFs and regulates both the pH-dependent dimerization of ANAC019$^{1–168}$ DBD monomers and transcription control of ANAC019 TF dimers. Are the reported changes in dimerization and DNA binding of ANAC019 physiologically relevant? We demonstrated that induction of ANAC083, one of ANAC019's target genes, was inhibited by ANAC019^{H135K} mutant protein, which is defect in dimerization and target binding. ANAC083 was reported to regulate xylem cell specification as transcription repressor (Yamaguchi et al., 2010). This implies that protonation on H135 of ANAC019 may affect the regulation of target genes and, hence, its biological function in plants. A similar case was reported for ARF5/MP protein, a DNA-binding auxin response factor (ARF). A mutation in the dimerization interface showed failure to complement the ARF5/MP mutant phenotypes (Boer et al., 2014).

We discovered that the removal of the C-domain of the ANAC019 TF abolished the pH dependency of the DNA-binding affinity of the ANAC019$^{1–168}$ DBD. We propose that the underlying mechanism for this phenomenon is that the long-range electrostatic interaction between DNA and the negatively charged C-terminal IDRs of a dimeric ANAC019 TF is responsible for the pH dependency of the binding affinity of the positively charged N-terminal DBD to DNA. It is important to recognize that for the 108 NAC TFs, the net charge of the N-terminal structured domains was mostly positive, whereas that of the C-terminal IDRs was mostly negative, with very few exceptions (Figure S4D). These data suggest that the functional modularity of the N-terminal DBD of a TF itself may not always be sufficient for its transcriptional control during changes in cellular pH but may require a negatively charged C-terminal IDR for turning on the pH dependency of the DNA-binding affinity of the N-terminal DBD. Therefore, the pH-tuned DNA-binding mechanism presented in this study could be a general mechanism for how a family of plant NAC TFs regulates their transcriptional function in response to a change in intracellular pH. This mechanism may provide a new perspective on the design principle of TFs in that the negatively charged IDR and positively charged DBD in a two-domain TF orchestrate transcriptional function.

EXPERIMENTAL PROCEDURES

Cloning and Expression of ANAC019$^{1–168}$

The ANAC019$^{1–168}$ DBD was first amplified by PCR with a TEV (tobacco etch virus nuclear inclusion) recognition site added at the N-terminal end. Amplified DNA was fused into the multiple cloning site [MCS] of the pET32a vector to obtain a TRX-tagged fusion protein. The construct was confirmed by sequencing of the plasmid. For our study, we first purified the protein as His-tagged fusion protein and later cleaved the tag using TEV protease and performed Ni-NTA column followed by size exclusion chromatography to separate the dimer and monomer forms of the protein. Plasmids were overexpressed in *Escherichia coli* strain BL21 (DE3), and positive colonies were selected on a Luria-Bertani (LB) plate with 0.1 mg/mL ampicillin. Induction was done using 1 mM IPTG (isopropyl-β-D-thiogalactopyranoside) at 0.5–0.6 optical density

(B) Three snapshots (A-, B-, and C-type) of ANAC019$^{1–317}$ full-length dimers and a snapshot (D-type dimer) of ANAC019$^{1–168}$ DBD without the C-domain. The φ dependence of the electrostatic interaction energy between A-, B, C-, or D-type dimers and DNA (bottom). We present only the case when $\theta = 0°$. The white region is the sterically forbidden region. The maximum orientational selectivity was achieved for the A-type when φ = 0°, 180°, or 360°, which refers to the binding configuration in PDB: 3SWP.
See also Figures S1 and S4.

600 (OD_{600}) and protein was overexpressed at 25°C at 160 rpm for 18 hr until OD_{600} > 1.5. Protein expression was confirmed using SDS-PAGE.

Purification of ANAC019$^{1–168}$

Cells containing fusion protein TRX-$His_{(6)}$-TEV-ANAC019$^{1–168}$ were sonicated in lysis buffer (25 mM NaPi, 300 mM NaCl, and 5 mM β-mercaptoethanol [pH 7.5]) containing a protease inhibitor cocktail (Roche, 50 μL). The lysate was centrifuged at 14,000 rpm for 30 min at 4°C. Recombinant TRX-fusion protein was purified by affinity chromatography on an Ni-NTA open column, washed with 20 mM imidazole in lysis buffer, and eluted with 500 mM imidazole in lysis buffer. Cleavage was performed overnight in lysis buffer with TEV protease to remove the TRX tag. The purity and identity of the protein were confirmed by SDS-PAGE analysis (12% or 15% gels). The presence of the target protein was confirmed by SDS-PAGE, which showed only one band of protein in the elution fraction. Further purification was carried by gel filtration chromatography in 20 mM sodium phosphate and 140 mM NaCl (pH 7.5) buffer on a Superdex 75 column.

$^{13}C/^{15}N$-Isotope Labeling of ANAC019$^{1–168}$

For heteronuclear NMR experiments, we prepared $^{13}C/^{15}N$-labeled ANAC019$^{1–168}$. Initially, cells were cultured in $^{12}C/^{14}N$ M9 minimal medium at 37°C and 220 rpm until the OD_{600} was 0.65. The cells were washed with PBS to remove all residual M9 medium and then centrifuged at 4,500 rpm at room temperature. The cell pellet was resuspended in $^{13}C/^{15}N$ isotope ($^{13}C/^{15}N$, 99%; Cambridge Isotope Laboratories) containing M9 media and maintained at an OD_{600} of 0.5–0.6. Induction was performed as described above. Cultured cells were harvested at 6,000 rpm for 30 min at 4°C. In addition, selective labeling was done as previously described (Tong et al., 2008) to confirm the resonance assignment of ANAC019$^{1–168}$.

NMR Spectroscopy for ANAC019$^{1–168}$

The NMR sample of ANAC019$^{1–168}$ (0.35 mM) was prepared in 20 mM sodium phosphate, 140 mM NaCl, 0.5 mM DTT, and 0.01% NaN_3 at either pH 7.5 or pH 6.0 and contained 10% D_2O. All NMR experiments were performed using the Bruker DRX 800MHz equipped with Cryoprobe. Backbone resonance assignment was performed by using standard double- and triple-resonance experiments (i.e., ^{1}H-^{15}N HSQC, HNCACB, HNCA, and CBCACONH) at 25°C. All spectra were analyzed and processed using XWINNMR (Bruker Biospin) and viewed using NMRpipe/NMRDraw software.

pH Titration of ANAC019$^{1–168}$ Using NMR

^{15}N-labeled ANAC019$^{1–168}$ was used for NMR titration at a final concentration of 0.3 mM. The titration was performed by changing the pH of ANAC019$^{1–168}$ from 7.5 to pH 6.0 after the initial ^{1}H-^{15}N HSQC experiment. Chemical shift perturbations were calculated using the equation $\Delta\delta_{av} = [(\Delta\delta_{1H})^2 + (\Delta\delta_{15N}/5)^2]^{1/2}$, where $\Delta\delta_{av}$, $\Delta\delta_{1H}$, and $\Delta\delta_{15N}$ are the average, proton, and ^{15}N chemical shift changes, respectively.

Transient Expression in *Arabidopsis* Protoplasts

Full-length ANAC019 and ANAC019^{H135K} cDNAs were fused to the HA epitope sequence in a plant-expression vector containing the 35SC4PPDK promoter and the nopaline synthase [NOS] terminator (Sheen, 1996). The ANAC019^{H135K} mutant clone was produced by QuikChange site-directed mutagenesis (Stratagene). All PCR products and mutations were confirmed by DNA sequencing. For luciferase reporter constructs, the promoter of ANAC083 was amplified from genomic DNA, cloned into pCR-CCD F (Kim and Somers, 2010), and recombined into the gateway version of the pGreen0800-LUC vector (Hellens et al., 2005), which contained 35Sp:RLuc (Renilla luciferase) as an internal control. *Arabidopsis* protoplasts were isolated and transfected as previously described (Hwang and Sheen, 2001). Transfected protoplasts were incubated for 6 hr at 22°C under dim light (5 $\mu E \cdot m^{-2} \cdot s^{-1}$), and luciferase activity was measured using a dual-luciferase reporter assay system according to the manufacturer's instructions (Promega).

Yeast Two-Hybrid Assays

The DupLEX-A system (OriGene) was used for yeast two-hybrid analysis of interactions. Full-length ANAC019, ANAC019^{H135K}, ANAC068, and ANAC068^{H132K} cDNAs were cloned into the pGilda bait vector, which produces an in-frame fusion with the LexA DBD, or into the pJG4-5 prey vector, which produces a B42 activation domain. The yeast strain EGY48 (*MATa*, *trp1*, *his3*, *ura3*, and *leu2*::6 LexAop-*LEU2*), which contains the *lacZ* reporter plasmid pSH18-34, was transformed with the appropriate "bait" and "prey" plasmids. Interactions were tested using 5-bromo-4-chloro-3-indolyl-β-D-galactopyranoside (X-gal) medium (Ryu et al., 2005).

Co-immunoprecipitation Assays

Full-length ANAC019 and ANAC019^{H135K} cDNAs and ANAC019 and ANAC019^{H135K} cDNA fragments encoding only the DBD were inserted into a plant expression vector that contained two copies of an HA or GFP tag driven by the *35SC4PPDK* promoter (Sheen, 1996). *Arabidopsis* mesophyll protoplasts were isolated from mature leaves of wild-type plants and transfected with various constructs expressing HA- or GFP-tagged proteins as previously described (Hwang and Sheen, 2001). Protoplasts were incubated overnight at 22°C under dim light (5 $\mu E \cdot m^{-2} \cdot s^{-1}$). Cells were harvested and lysed with IP buffer (50 mM Tris-HCl [pH 7.5], 150 mM NaCl, 10 mM EDTA, 0.1% Nonidet P-40, 50 μM MG132, 1 mM PMSF, and protease inhibitor cocktail). The supernatant was incubated with an agarose-conjugated anti-GFP antibody (GFP-Trap, ChromoTek) for 2 hr at 4°C. The pellet fraction was washed four times with 50 mM Tris-HCl (pH 7.5), 150 mM NaCl, 10 mM EDTA, 0.1% Nonidet P-40, and protease inhibitor cocktail. The protein extracts and immunoprecipitated samples were heated at 95°C for 5 min in SDS-PAGE sample loading buffer, separated on 10% SDS-PAGE gels, and transferred to polyvinylidene fluoride (PVDF) membranes. The blot was probed first with horseradish peroxidase (HRP)-conjugated monoclonal anti-HA (Santa Cruz Biotechnology) antibody and then stripped with 0.2 N glycine (pH 3.0) and reprobed with HRP-conjugated monoclonal anti-GFP (Santa Cruz Biotechnology) antibody.

Size Exclusion Gel Chromatography Assay

ANAC019$^{1–168}$ was purified using Ni-NTA affinity chromatography. The molecular mass and folded state of the protein were analyzed by size exclusion chromatography with HiLoad Superdex 200 and 75 columns (Pharmacia) in buffer containing 20 mM sodium phosphate. The Superdex 200 column was used for 140 mM and 57 mM NaCl conditions. To determine the exact intensity related to the ratio between monomer and dimer concentrations in 70 mM NaCl, the Superdex 75 column was used. Molecular weight was calculated using the equations $y = -1.6319x + 7.6534$ for Superdex 200 and $y = -1.2507x + 6.2898$ for Superdex 75, where x represents the Ve/Vo, (Ve = elution volume, Vo = void volume; 47.432 mL and 46.609 mL for Superdex 200 and 75, respectively). Molecular mass was calculated against the standard proteins albumin (66 kDa), carbonic anhydrase (29 kDa), cytochrome *c* (12.4 kDa), and aprotinin (6.5 kDa).

EMSA

A double-stranded oligonucleotide containing an optimized palindromic version of the NAC-binding site (NAC-BS) (Jensen et al., 2010) was prepared by annealing complementary single-stranded oligonucleotides of the sequence 5′-CAGTCTTGCGTGTTGGAACACGCAACAGTC-3′. The double-stranded oligonucleotide was labeled at the 3′ end with DIG (digoxigenin) using a DIG gel-shift kit (second generation; Roche). The DNA-binding reactions contained 4 μL 5 × binding buffer (100 mM sodium phosphate buffer [pH 7.0, 6.5, and 6.0], which consisted of 5 mM EDTA, 50 mM $(NH_4)_2SO_4$, 5 mM DTT, 1% (w/v) Tween-20, 150 mM KCl, and 1 μg poly[d(I-C)]), 31 fmol DIG-labeled DNA and 100 ng full-length ANAC019$^{1–317}$, full-length ANAC019^{H135K}, or ANAC019$^{1–168}$ DBD recombinant protein in a final volume of 20 μL. For the competition assay, 4 pmol unlabeled DNA was added. The binding reactions were incubated for 15 min at room temperature (20°C) and separated by PAGE (10% PAGE gold precast gels; Cambrex). Electroblotting was performed using a Hybond-N nylon membrane (Amersham Biosciences), and chemiluminescent detection was carried out according to the manufacturer's instructions.

All-Atom MD Simulation

All-atom MD simulations on ANAC019 were performed using PMEMD.CUDA in the AMBER12 MD simulation package with the ff99SB force field. For a more detailed description, see Supplemental Experimental Procedures.

SUPPLEMENTAL INFORMATION

Supplemental Information includes Supplemental Experimental Procedures, four figures, and one table and can be found with this article online at https://doi.org/10.1016/j.celrep.2018.01.002.

ACKNOWLEDGMENTS

This work was funded by the Creative Research Initiatives of the National Research Foundation (NRF) of Korea (2008-0061984 to M.K., S.K., and I.C.) and the DGIST Core Protein Resources Center (N0001822 to I.C.). H.J.K., B.-K.P., and H.G.N. were supported by the Institute for Basic Science (IBS-R013-D1). J.-h.Y., P.S., and W.L. were supported by Mid-career Researcher Program (2017R1A2B2008483 to W.L.) and Basic Science Research Program (2016R1A6A3A04010213 to J.-h.Y.) of NRF. We acknowledge the DGIST Supercomputing and Big Data Center for the dedicated allocation of supercomputing time.

AUTHOR CONTRIBUTIONS

W.L., H.G.N., and I.C. conceived the idea and designed the research. M.K and S.K performed structural modeling, MD simulations, protein-protein docking, and protein-DNA interaction analysis. H.J.K. and B.-K.P performed transient expression, yeast two-hybrid and co-immunoprecipitation assays, and EMSA experiments. P.S. and J.-h.Y. performed cloning, purification, size exclusion chromatography, labeling, and NMR experiments. W.L., H.G.N., and I.C. wrote the paper.

DECLARATION OF INTERESTS

The authors declare no competing interests.

Received: August 9, 2017
Revised: December 12, 2017
Accepted: December 28, 2017
Published: January 30, 2018

REFERENCES

Bista, M., Freund, S.M., and Fersht, A.R. (2012). Domain-domain interactions in full-length p53 and a specific DNA complex probed by methyl NMR spectroscopy. Proc. Natl. Acad. Sci. USA *109*, 15752–15756.

Boer, D.R., Freire-Rios, A., van den Berg, W.A., Saaki, T., Manfield, I.W., Kepinski, S., López-Vidrieo, I., Franco-Zorrilla, J.M., de Vries, S.C., Solano, R., et al. (2014). Structural basis for DNA binding specificity by the auxin-dependent ARF transcription factors. Cell *156*, 577–589.

Ernst, H.A., Olsen, A.N., Larsen, S., and Lo Leggio, L. (2004). Structure of the conserved domain of ANAC, a member of the NAC family of transcription factors. EMBO Rep. *5*, 297–303.

Filtz, T.M., Vogel, W.K., and Leid, M. (2014). Regulation of transcription factor activity by interconnected post-translational modifications. Trends Pharmacol. Sci. *35*, 76–85.

Hellens, R.P., Allan, A.C., Friel, E.N., Bolitho, K., Grafton, K., Templeton, M.D., Karunairetnam, S., Gleave, A.P., and Laing, W.A. (2005). Transient expression vectors for functional genomics, quantification of promoter activity and RNA silencing in plants. Plant Methods *1*, 13.

Hwang, I., and Sheen, J. (2001). Two-component circuitry in Arabidopsis cytokinin signal transduction. Nature *413*, 383–389.

Jensen, M.K., Kjaersgaard, T., Nielsen, M.M., Galberg, P., Petersen, K., O'Shea, C., and Skriver, K. (2010). The Arabidopsis thaliana NAC transcription factor family: structure-function relationships and determinants of ANAC019 stress signalling. Biochem. J. *426*, 183–196.

Kim, J., and Somers, D.E. (2010). Rapid assessment of gene function in the circadian clock using artificial microRNA in Arabidopsis mesophyll protoplasts. Plant Physiol. *154*, 611–621.

Kim, J.H., Woo, H.R., Kim, J., Lim, P.O., Lee, I.C., Choi, S.H., Hwang, D., and Nam, H.G. (2009). Trifurcate feed-forward regulation of age-dependent cell death involving miR164 in Arabidopsis. Science *323*, 1053–1057.

Kragelund, B.B., Jensen, M.K., and Skriver, K. (2012). Order by disorder in plant signaling. Trends Plant Sci. *17*, 625–632.

Mikles, D.C., Bhat, V., Schuchardt, B.J., Deegan, B.J., Seldeen, K.L., McDonald, C.B., and Farooq, A. (2013). pH modulates the binding of early growth response protein 1 transcription factor to DNA. FEBS J. *280*, 3669–3684.

Müller, C.W. (2001). Transcription factors: global and detailed views. Curr. Opin. Struct. Biol. *11*, 26–32.

Olsen, A.N., Ernst, H.A., Lo Leggio, L., Johansson, E., Larsen, S., and Skriver, K. (2004). Preliminary crystallographic analysis of the NAC domain of ANAC, a member of the plant-specific NAC transcription factor family. Acta Crystallogr. D Biol. Crystallogr. *60*, 112–115.

Ooka, H., Satoh, K., Doi, K., Nagata, T., Otomo, Y., Murakami, K., Matsubara, K., Osato, N., Kawai, J., Carninci, P., et al. (2003). Comprehensive analysis of NAC family genes in Oryza sativa and Arabidopsis thaliana. DNA Res. *10*, 239–247.

Ryu, J.S., Kim, J.I., Kunkel, T., Kim, B.C., Cho, D.S., Hong, S.H., Kim, S.H., Fernández, A.P., Kim, Y., Alonso, J.M., et al. (2005). Phytochrome-specific type 5 phosphatase controls light signal flux by enhancing phytochrome stability and affinity for a signal transducer. Cell *120*, 395–406.

Sheen, J. (1996). Ca2+-dependent protein kinases and stress signal transduction in plants. Science *274*, 1900–1902.

Spitz, F., and Furlong, E.E. (2012). Transcription factors: from enhancer binding to developmental control. Nat. Rev. Genet. *13*, 613–626.

Tong, K.I., Yamamoto, M., and Tanaka, T. (2008). A simple method for amino acid selective isotope labeling of recombinant proteins in E. coli. J. Biomol. NMR *42*, 59–67.

Welner, D.H., Lindemose, S., Grossmann, J.G., Møllegaard, N.E., Olsen, A.N., Helgstrand, C., Skriver, K., and Lo Leggio, L. (2012). DNA binding by the plant-specific NAC transcription factors in crystal and solution: a firm link to WRKY and GCM transcription factors. Biochem. J. *444*, 395–404.

Yamaguchi, M., Ohtani, M., Mitsuda, N., Kubo, M., Ohme-Takagi, M., Fukuda, H., and Demura, T. (2010). VND-INTERACTING2, a NAC domain transcription factor, negatively regulates xylem vessel formation in Arabidopsis. Plant Cell *22*, 1249–1263.